NANOSYSTEMS: PHYSICS, CHEMISTRY, MATHEMATICS, 2014, 5 (2), P. 234–248

LOCALIZED STATES AND STORAGE OF OPTICAL INFORMATION UNDER THE QUBIT-LIGHT INTERACTION IN MICRO-SIZE CAVITY ARRAYS

[1]E. S. Sedov, [1]S. M. Arakelian, [1,2]A. P. Alodjants

[1] Department of Physics and Applied Mathematics, Vladimir State University named after A. G. and N. G. Stoletovs, Gorky Street 87, RU-600000, Vladimir, Russia
[2] Russian Quantum Center, 100 Novaya str., Skolkovo, Moscow region, 143025, Russia
alodjants@vlsu.ru

PACS 42.50.Pq, 05.45.Yv, 42.50.Ex, 71.36.+c

We suggest the model of lattice low branch (LB) polaritons based on the array of weakly coupled micro-size cavities, each containing a small but macroscopic number of two-level systems (qubits). We reveal various dynamical regimes, such as diffusive, self-trapped, breathing and solitonic for polariton wave packet propagation under tight-binding approximation. We focus our attention on the bright polariton soliton formation in a high quality cavity array emerging due to two-body polariton-polariton scattering processes that take place at each cavity under the qubit-light interaction. A physical algorithm for the spatially distributed storage of optical information where various dynamical LB polariton soliton states are used is proposed. This algorithm can be realized with the help of manipulating group velocity of a polariton soliton in the cavity array and obtained by smooth variation of qubit-light detuning.

Keywords: polariton, quantum information, qubit, soliton, spatially-periodic structure.

1. Introduction

The current remarkable achievements with trapped atomic gases, semiconductor technologies and photonic crystal devices represent important progress towards solving problems for the design of novel devices operating at the quantum level of matter-light field interaction [1]. In particular, memory devices recently proposed in quantum physics for the above purposes explore different methods for the entanglement of atoms (or two- or multi-level oscillators) with quantized electromagnetic fields and mapping of the quantum state of light onto matter by using slow light phenomenon [2]. Physically, various quantum optical memory protocols, widely discussed now for different types of interaction of quantized light field with two or multi-level atoms are linear (see, e.g. [1, 3]) as rule, and based on linear coupling between matter excitations and quantized field. Actually, they can be realized in very dilute atomic gases [4]. In this sense, the processes occurring in the systems as well as relevant quantum optical memory protocols can be explained in a very elegant way by using polaritons representing a linear superposition of a quantized field and collective excitations in matter, [5]. In this case, the essential reduction of the group velocity of an optical pulse emerging in the atomic medium, under EIT effect as an example, may be controlled by a pump field and can be explained by polariton transformation in the medium. More precisely, the group velocity of light in this limit is determined by the velocity of atom-like polaritons that could be low enough due to large polariton mass that is $m_{\rm pol} \simeq m_{\rm at}$, cf. [6].

However, this simple physical picture, as well as quantum memory protocols, requires essential clarification if we deal with optical pulse propagation in lattice structures.

It is worth noting that at present, various lattice models of qubit-light interaction of different dimensionality represent an important tool to provide quantum information storage and processing within the framework of modern scalable quantum technologies, cf. [7, 8]. In this sense, it seems promising to exploit cavity arrays (or 2D lattices) containing two-level systems (atoms, quantum dots, Cooper pair boxes) strongly interacting with the cavity field at each site [9, 10]. Addressability and controlling of qubits at each cavity make such systems good candidates for quantum computing [11]. Thus, if we speak about the properties of the group velocity of polaritons in a lattice system, we should take into account the fact that the group velocity in the lattices is strongly modified within the Brillouin zone [12].

Nonlinear effects become important under the strong matter-field interaction in semiconductor microstructures. Recently, macroscopic coherent effects such as polariton lasing and superfluidity have been observed for low-branch (LB) exciton-polaritons in semiconductor quantum well structures embedded in Bragg microcavities [13–15]. In such systems, strong Kerr-like nonlinearity caused by two-body polariton-polariton interaction leads to the formation of bright polariton solitons, even for a small number of particles; this open new perspectives for storing and processing quantum information, cf. [16].

Thus, in solid state systems the behavior of a coupled matter-field state is connected with the interplay between dispersion characteristics and strong nonlinearity. In this sense, it seems to be important and useful to refer to the problem of dynamical phases of atomic Bose-Einstein condensates (BEC) confined in a deep optical lattice potential [17, 18]. In particular, it is shown that intrinsically localized excitations, such as breathers and/or solitons, as well as self-trapping and diffusive regimes can exist in the presence of a repulsive atom-atom interaction.

In the present paper, we continue our theoretical investigation of mean field collective properties of coupled atom-light states – LB polaritons emerging due to the interaction of two-level systems (qubits) with a single-mode optical field in a cavity array, [19]. In previous work, we reveal the existence of bright polariton soliton solutions by using the complex Ginzburg-Landau equation that was derived in the continuum limit, taking into account the effects of cavity field dissipation and qubit dephasing [20]. Although we suggested rubidium atoms for numerical simulations, our model could be applied to different qubit systems, such as quantum dots, Cooper pair boxes, etc. One of the main features of our approach is strong nonlinearity which occurs due to small cavity volumes occupied by optical field, that is $V \simeq (\lambda/2n)^3$, where λ is light wavelength, n is refractive index. Current nanotechnologies enable the design of such cavities by using, for example, defects in semiconductor membranes, representing 2D photonic crystals [21], or cavities with whispering gallery modes [22]. In this paper, we consider a tight-binding model that includes neighbor hopping effects for photonic fields. This model leads to strong photonic correlations and nonlinear properties for coupled matter-field states in the lattice. In practice, small period 1D lattices could be created by using silicon heterostructures [23] or by a waveguide array [24].

The paper is arranged as follows: in Sec. 2, we explain in detail our model where qubit-light interaction in a cavity array is realized at microscales. In this case, a tight-binding model will be established. In Sec. 3, we introduce a coupled qubit-light excitation basis for our system. Apart from the results obtained previously (see e.g. [20]), LB polaritons emerging at each site of the cavity array are the subject of our study in the rest of the paper. In order, to obtain polariton wave packet behavior in the QED cavity array, we use a time dependent variational approach. Basic equations for the wave packet parameters

and their general properties are established in Sec. 4. The main results of the paper are given in Sec. 5 and relay to investigation of 1D lattice polariton wave packet dynamical regimes. In Sec. 6 we propose a novel algorithm of storing of optical information by using lattice polariton solitons. In the conclusion, we summarize the results obtained. In the Appendix we discuss realistic properties of cavity-QED array parameters for two-level rubidium atoms chosen as a qubit system and interacting with an optical field.

2. Qubit-light interaction model

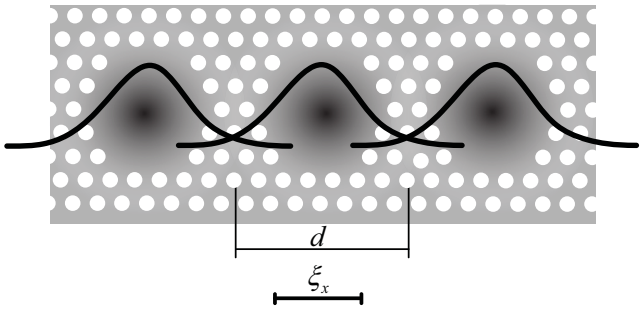

Fig. 1. Schematic for the proposed 1D cavity QED arrays, where each cavity contains an ensemble of two-level systems (TLS) – qubits. Parameter d represents the size of the cavity, ξ_x is characteristic spatial scale of the optical field localization. The shaded region in the center of each cavity depicts the TLS wave function of scale σ_x. In the paper we assume that $\sigma_x < \xi_x \leqslant d$

We consider a one-dimensional (1D) array of small (microscale) cavities, each containing an ensemble of small but macroscopic number N_n of interacting two-level systems (TLS) – qubits, see Fig. 1. The total Hamiltonian $\hat{H}$ for the qubit–light coupled system in Fig. 1 can be represented as:

$$\hat{H} = \hat{H}_{\rm TLS} + \hat{H}_{\rm PH} + \hat{H}_{\rm I}, \tag{1}$$

where $\hat{H}_{\rm TLS}$ is a quantum field theory Hamiltonian for *noninteracting* qubits, $\hat{H}_{\rm PH}$ is responsible for the photonic field distribution, and term $\hat{H}_{\rm I}$ characterizes the qubit-light interaction in each cavity. The parts of the total Hamiltonian can be written in the second quantized form as:

$$\hat{H}_{\rm TLS} = \sum_{\substack{i,j=1,2 \\ i\neq j}} \int \hat{\Phi}_j^{\dagger} \left(-\frac{\hbar^2 \Delta}{2M_{\rm at}} + V_{\rm ext}^{(j)} \right) \hat{\Phi}_j d\vec{r}, \tag{2}$$

$$\hat{H}_{\rm PH} = \int \hat{\Phi}_{\rm ph}^{\dagger} \left(-\frac{\hbar^2 \Delta}{2M_{\rm ph}} + V_{\rm ph} \right) \hat{\Phi}_{\rm ph} d\vec{r}, \tag{3}$$

$$\hat{H}_{\rm I} = \hbar\kappa \int \left(\hat{\Phi}_{\rm ph}^{\dagger} \hat{\Phi}_1^{\dagger} \hat{\Phi}_2 + \hat{\Phi}_2^{\dagger} \hat{\Phi}_1 \hat{\Phi}_{\rm ph} \right) d\vec{r}, \tag{4}$$

where $M_{\rm at}$ is a mass of free two-level particles, $M_{\rm ph}$ is a mass of trapped photons. In (2) – (4), quantum field operators $\hat{\Phi}_{1,2}(\vec{r})$, $\hat{\Phi}_{1,2}^{\dagger}(\vec{r})$ ($\hat{\Phi}_{\rm ph}(\vec{r})$, $\hat{\Phi}_{\rm ph}^{\dagger}(\vec{r})$) annihilate and create particles (photons) at position $\vec{r}$; $V_{\rm ext}^{(j)}$ $(j = 1, 2)$, and $V_{\rm ph}$ are trapping potentials for TLS and photons, respectively.

In general, one can expand atomic ($\hat{\Phi}_j$) and photonic ($\hat{\Phi}_{\rm ph}$) field operators as follows:

$$\hat{\Phi}_j(\vec{r}) = \sum_n \hat{a}_{j,n}\varphi_{j,n}(\vec{r}), \qquad \hat{\Phi}_{\rm ph}(\vec{r}) = \sum_n \hat{\psi}_n \xi_n(\vec{r}), \quad j = 1, 2, \tag{5}$$

where wave functions $\varphi_{j,n}(\vec{r})$, $\xi_n(\vec{r})$ are real (Wannier) functions responsible for the spatial distribution of qubits and photons at n–site. They fulfill a normalization condition $\int_{-\infty}^{+\infty}(\varphi_{j,n}(\vec{r}))^2 d\vec{r} = \int_{-\infty}^{+\infty}(\xi_n(\vec{r}))^2 d\vec{r} = 1$. In the Appendix, we use a variational Gaussian ansatz approach for estimating $\varphi_{j,n}(\vec{r})$, $\xi_n(\vec{r})$ functions.

Annihilation operators $\hat{a}_{1,n}$ and $\hat{a}_{2,n}$ in (5) characterize the dynamical properties of qubit ensembles (quantum modes) at internal lower ($|1\rangle$) and upper ($|2\rangle$) levels, respectively. Annihilation operator $\hat{\psi}_n$ in (5) describes the temporal behavior of a photonic mode located at the nth lattice cavity. Substituting (5) for (2)–(4) one can obtain:

$$\hat{H}_{\rm TLS} = \hbar \sum_{j=1}^{2}\sum_{n}^{M}\left[\omega_n^{(j)}\hat{a}_{j,n}^{\dagger}\hat{a}_{j,n} - \beta_{j,n}\left(\hat{a}_{j,n}^{\dagger}\hat{a}_{j,n+1} + \hat{a}_{j,n}^{\dagger}\hat{a}_{j,n-1}\right)\right], \tag{6}$$

$$\hat{H}_{\rm PH} = \hbar \sum_{n}^{M}\left[\omega_{n,\,\rm ph}\hat{\psi}_n^{\dagger}\hat{\psi}_n - \alpha_n\left(\hat{\psi}_n^{\dagger}\hat{\psi}_{n+1} + \hat{\psi}_n^{\dagger}\hat{\psi}_{n-1}\right)\right], \tag{7}$$

$$\hat{H}_{\rm I} = \hbar \sum_{n}^{M}\frac{g}{\sqrt{N_n}}\left[\hat{\psi}_n^{\dagger}\hat{a}_{1,n}^{\dagger}\hat{a}_{2,n} + \hat{a}_{2,n}^{\dagger}\hat{a}_{1,n}\hat{\psi}_n\right], \tag{8}$$

where $N_n = \hat{a}_{1,n}^{\dagger}\hat{a}_{1,n} + \hat{a}_{2,n}^{\dagger}\hat{a}_{2,n}$ is an operator of a total number of TLS at nth lattice cell. Frequencies $\omega_n^{(j)}$, $\omega_{n,\,\rm ph}$ and hopping constants $\beta_{j,n}$, α_n look like:

$$\omega_n^{(j)} = \frac{1}{\hbar}\int\left(\frac{\hbar^2}{2M_{\rm at}}(\vec{\nabla}\varphi_{j,n})^2 + \varphi_{j,n}V_{\rm ext}^{(j)}\varphi_{j,n}\right)d\vec{r}, \tag{9}$$

$$\omega_{n,\rm ph} = \frac{1}{\hbar}\int\left(\frac{\hbar^2}{2M_{\rm at}}(\vec{\nabla}\xi_n)^2 + \xi_n V_{\rm ph}\xi_n\right)d\vec{r}, \tag{10}$$

$$\beta_{j,n} = -\frac{1}{\hbar}\int\left(\frac{\hbar^2}{2M_{\rm at}}\vec{\nabla}\varphi_{j,n}\cdot\vec{\nabla}\varphi_{j,n+1} + \varphi_{j,n}V_{\rm ext}^{(j)}\varphi_{j,n+1}\right)d\vec{r}, \tag{11}$$

$$\alpha_n = -\frac{1}{\hbar}\int\left[\frac{\hbar^2}{2M_{\rm ph}}\vec{\nabla}\xi_n\cdot\vec{\nabla}\xi_{n+1} + \xi_n V_{\rm ph}\xi_{n+1}\right]d\vec{r}, \tag{12}$$

$$g = \kappa\int\xi_n\varphi_{1,n}\varphi_{2,n}d\vec{r}. \tag{13}$$

Thereafter, we assume for simplicity that all cavities are identical to each other and contain the same average number $N = \langle N_n\rangle$ of qubits. In this case, it is convenient to suppose that functions $\varphi_{j,n}(\vec{r})$ are identical for all n, that is $\varphi_{j,n}(\vec{r}) \simeq \varphi_{j,n\pm1}(\vec{r})$.

Parameter $\alpha_n \equiv \alpha$ in (12) describes overlapping of the optical field for nearest-neighbor cavities. Coupling coefficients $\beta_{j,n} \equiv \beta_j$ in (11) are hopping constants for qubits in the 1D lattice structure.

3. Polaritons in the cavity array

Now, we use the Schwinger representation to describe a matter-field interaction and introduce TLS excitation operators $\hat{S}_{+,\,n} = \hat{a}_{2,n}^{\dagger}\hat{a}_{1,n}$, $\hat{S}_{-,\,n} = \hat{a}_{1,n}^{\dagger}\hat{a}_{2,n}$ and population imbalance operator $\hat{S}_{z,\,n} = \frac{1}{2}\left(\hat{a}_{2,n}^{\dagger}\hat{a}_{2,n} - \hat{a}_{1,n}^{\dagger}\hat{a}_{1,n}\right)$. Then, we map the operators onto the atomic

excitation operators $\hat{\phi}_n$, $\hat{\phi}_n^\dagger$, applying the so-called Holstein–Primakoff transformation:

$$\hat{S}_{+,n} = \hat{\phi}_n^\dagger \sqrt{N - \hat{\phi}_n^\dagger \hat{\phi}_n}, \quad \hat{S}_{-,n} = \sqrt{N - \hat{\phi}_n^\dagger \hat{\phi}_n}\,\hat{\phi}_n, \quad \hat{S}_{z,n} = \hat{\phi}_n^\dagger \hat{\phi}_n - N/2. \tag{14}$$

It is worth noting that atomic excitation operators $\hat{\phi}_n$, $\hat{\phi}_n^\dagger$ obey usual bosonic commutation relations $\left[\hat{\phi}_n, \hat{\phi}_m^\dagger\right] = \delta_{mn}$. Strictly speaking, it is possible to treat the operators $\hat{a}_{1,n}$ and $\hat{a}_{2,n}$ describing particles at lower and upper levels respectively, as $\hat{a}_{1,n} \approx \sqrt{N} - \frac{\hat{\phi}_n^\dagger \hat{\phi}_n}{2N^{1/2}}$, cf. [19].

Thus, if number N at each cavity is macroscopic, but not so large, one can keep all the terms in expansion of $\hat{a}_{1,n}$. In this limit, for Hamiltonian $\hat{H} = \hat{H}_{\rm L} + \hat{H}_{\rm C} + \hat{H}_{\rm NL}$, we obtain the following:

$$\hat{H}_{\rm L} = \hbar \sum_n \left[\tilde{\omega}_{12} \hat{\phi}_n^\dagger \hat{\phi}_n + \omega_{n,\,\rm ph} \hat{\psi}_n^\dagger \hat{\psi}_n + g \left(\hat{\psi}_n^\dagger \hat{\phi}_n + H.C. \right) \right], \tag{15}$$

$$\hat{H}_{\rm C} = -\hbar \sum_n \left[\beta \hat{\phi}_n^\dagger \hat{\phi}_{n+1} + \alpha \hat{\psi}_n^\dagger \hat{\psi}_{n+1} + H.C. \right], \tag{16}$$

$$\hat{H}_{\rm NL} = -\hbar \sum_n \left[\frac{g}{2N} \left(\hat{\psi}_n^\dagger \hat{\phi}_n^\dagger \hat{\phi}_n^2 + H.C. \right) \right], \tag{17}$$

where we have introduced new parameters $\tilde{\omega}_{12} = \omega_n^{(2)} - \omega_n^{(1)} + 2\beta_{1,n}$, $\beta = \beta_2$.

Let us introduce lattice polariton operators as follows:

$$\hat{\Xi}_{1,n} = X_n \hat{\psi}_n + C_n \hat{\phi}_n, \qquad \hat{\Xi}_{2,n} = X_n \hat{\phi}_n - C_n \hat{\psi}_n, \tag{18}$$

where X_n and C_n are Hopfield coefficients defined as:

$$\begin{pmatrix} X_n \\ C_n \end{pmatrix} = \frac{1}{\sqrt{2}} \left(1 \pm \frac{\delta_n}{\sqrt{4g^2 + \delta_n^2}} \right)^{1/2}. \tag{19}$$

In Eq. (19), $\delta_n = \omega_{n,\,\rm ph} - \tilde{\omega}_{12}$ is a qubit-light field detuning chosen at each cavity. Note that parameters X_n and C_n are considered equivalent for all cavities (sites n), assuming that $X \equiv X_n$ and $C \equiv C_n$. This approach implies equal qubit-light detuning $\delta = \delta_n$ for all cavities as well.

Operators $\hat{\Xi}_{1,n}$ and $\hat{\Xi}_{2,n}$ in (18) characterize two types of Bose-quasiparticles, i.e. upper and lower branch polaritons occurring at each site of the lattice due to the matter–field interaction. At the low density limit, Eqs. (18) and (19) represent the exact solution that diagonalizes a linear part $\hat{H}_{\rm L}$ of the total Hamiltonian $\hat{H}$.

At equilibrium, the lowest polariton branch is much more heavily populated. Here, we use a mean-field approach to replace the corresponding polariton field operator $\hat{\Xi}_n$ with its average value $\left\langle \hat{\Xi}_n \right\rangle$, which simply characterizes the LB polariton wave function at the nth cavity. For further processing, we introduce the nth normalized polariton amplitude as $\Psi_n = \left\langle \hat{\Xi}_n \right\rangle / \sqrt{N_{\rm pol}}$, where $N_{\rm pol} = \sum_n \left\langle \hat{\Xi}_n^\dagger \hat{\Xi}_n \right\rangle$ is the total number of LB polaritons at the array. Under this approach, substituting (18) for (15)–(17) and keeping LB polariton terms only, we arrive at:

$$H = \hbar \sum_n^M \left[\Omega_{\rm LB} \left| \Psi_n \right|^2 - \Omega_{\rm T} \left(\Psi_n^* \Psi_{n+1} + C.C. \right) + \frac{1}{2} \Omega_{\rm I} \left| \Psi_n \right|^4 \right], \tag{20}$$

where we have introduced characteristic frequency $\Omega_{\rm LB}$, polariton tunneling rate $\Omega_{\rm T}$ and interaction strength $\Omega_{\rm I}$ as follows:

$$\Omega_{\rm LB}=\frac{1}{2}\left(\tilde{\omega}_{12}+\omega_{n,\,\rm ph}-\sqrt{\delta^2+4g^2}\right),\quad \Omega_{\rm T}=\beta X^2+\alpha C^2,\quad \Omega_{\rm I}=2gCX^3\frac{N_{\rm pol}}{N}. \tag{21}$$

Actually, in the limit of negative and large qubit-light field detuning chosen as $|\delta|\gg g$, $\delta<0$ ($X\simeq g/|\delta|, C\simeq 1$), the LB polaritons behave as photons, i.e. $\Xi_{2,n}\simeq\psi_n$. Thus, we can represent the frequency parameters as $\Omega_{\rm LB}\simeq\omega_{\rm ph}$, $\Omega_{\rm T}=\alpha$, $\Omega_{\rm I}=2N_{\rm pol}g^4/N|\delta|^3$.

In another limit, we can take $|\delta|\gg g$, $\delta>0$ ($X\simeq 1$, $C\simeq g/\delta$) and then LB polaritons behave as excited atoms, i.e. $\Xi_{2,n}\simeq\phi_n$. We readily find for the coefficients $\Omega_{\rm LB}\simeq\tilde{\omega}_{12}$, $\Omega_{\rm T}=\beta+\alpha\frac{g^2}{\delta^2}$, $\Omega_{\rm I}=\frac{2g^2}{\delta}\frac{N_{\rm pol}}{N}$.

4. Time-dependent variational approach

To analyze different regimes of polaritons in the lattice, we study the dynamical evolution of in-site Gaussian shape wave packet, which we represent as:

$$\Psi_n=\quad \mathbb{N}\exp\left[-\frac{(x-{\rm X}(t))^2}{\Gamma(t)^2}+ik(t)(x-{\rm X}(t))+i\frac{\theta(t)}{2}(x-{\rm X}(t))^2\right], \tag{22}$$

where $X(t)$ and $\Gamma(t)$ are a time dependent center and a width of the wave packet, respectively, $k(t)$ is momentum and $\theta(t)$ is curvature, $\mathbb{N}=\left(\sqrt{2}/\sqrt{\pi}\Gamma(t)\right)^{1/2}$ is a normalization constant (the wave packet amplitude). Lattice coordinate x relays to the number of sites (cavities) n as $x=nd$. The wave packet dynamical evolution can be obtained in accordance with a variational principle from the Lagrangian density:

$$L=\hbar\sum_n^M\left[\frac{i}{2}\left(\Psi_n^*\frac{\partial\Psi_n}{\partial t}-\Psi_n\frac{\partial\Psi_n^*}{\partial t}\right)-\Omega_{\rm LB}\,|\Psi_n|^2+\Omega_{\rm T}\left(\Psi_n^*\Psi_{n+1}+C.C.\right)-\frac{1}{2}\Omega_{\rm I}|\Psi_n|^4\right]. \tag{23}$$

Plugging Eq. (22) into Eq. (23), it is possible to calculate the effective Lagrangian $\bar{L}$ by averaging the Lagrangian density (23), as

$$\bar{L}=\quad \hbar\left[k\dot{X}-\frac{\dot{\theta}\Gamma^2}{8}+2\Omega_{\rm T}\cos(kd)\,e^{-\sigma}-\frac{\Omega_{\rm I}d}{2\Gamma\sqrt{\pi}}\right], \tag{24}$$

where we gave the following denotation $\sigma=\frac{\Gamma^2\theta^2d^2}{8}+\frac{d^2}{2\Gamma^2}$. Noting that Eq. (24) is valid when parameter Γd is not too small, that is $\Gamma d\geqslant 1$, cf. [17,18].

Using Lagrangian (24), one can obtain the following variational equations for the canonically conjugate polariton wave packet parameters:

$$\dot{k}=0,\quad \dot{X}=2d\Omega_{\rm T}\sin(kd)\,e^{-\sigma},\quad \dot{\Gamma}=\frac{\hbar\Gamma\theta}{M^*},\quad \dot{\theta}=\frac{\hbar}{M^*}\left(\frac{4}{\Gamma^4}-\theta^2\right)+\frac{2\Omega_{\rm I}d}{\sqrt{\pi}\Gamma^3}. \tag{25}$$

In Eq. (25), we also introduced an effective polariton mass in the lattice

$$M^*=\frac{1}{\hbar^2}\frac{\partial^2H}{\partial k^2}=\frac{m_{\rm ex}m_{\rm ph}}{m_{\rm ex}C^2+m_{\rm ph}X^2}, \tag{26}$$

for which we use the definition of photon $m_{\rm ph}=\hbar e^{\sigma}\sec(kd)/2d^2\alpha$ and qubit exciton $m_{\rm ex}=\hbar e^{\sigma}\sec(kd)/2d^2\beta$ masses in the lattice respectively. In Eq. (26) H is the Hamiltonian for

the system (25) that looks like:

$$H = -\frac{\hbar^2}{d^2 M^*} + \frac{\hbar \Omega_{\mathrm{I}} d}{2\sqrt{\pi}\Gamma}. \tag{27}$$

Using Eq. (26) for the group velocity of a polariton wave packet one can obtain

$$v_g \equiv \frac{1}{\hbar}\frac{\partial H}{\partial k} = \dot{\mathrm{X}} = \frac{\hbar}{d}\frac{\tan(kd)}{M^*}. \tag{28}$$

The first equation in (25) implies that the momentum of a polariton wave packet is preserved in time, i.e. $k(t)|_{t=0} \equiv k_0$. Hence, we are able to consider the properties of a polariton wave packet by fixing initial value of momentum k. For a small momentum such as $kd \ll 1$, which is typically associated with the middle area of the Brillouin zone from Eqs. (26) and (28), one can obtain a convenient result for the polariton group velocity, that is $v_g \approx \frac{\hbar k}{M^*}$, where $M^* \simeq \hbar e^{\sigma}/2d^2\Omega_{\mathrm{T}}$.

In this paper, we are interested mainly in the polaritons with large and negative effective mass M^*. Practically, in this case we anticipate slow soliton regimes for a polariton wave packet spreading in the lattice.

The maximal negative polariton mass $M_0^* = -\hbar e^{\sigma}/2d^2\Omega_{\mathrm{T}}$ can be obtained at $\cos(kd) = -1$ that corresponds to the edge of the Brillouin zone, cf. [19]. Obviously, the group velocity of a polariton wave packet vanishes, i.e. $v_g = 0$.

For further analysis, it is also fruitful to rewrite Eq. (25) introducing dimensionless variables $p = kd$, $\xi = X/d$, $\gamma = \Gamma/d$ and $\eta = \theta d^2$. In this case, the set of Eq. (25) takes the form of:

$$\dot{\xi} = \omega_{\mathrm{T}} \sin(p)\, e^{-\sigma}, \quad \dot{\gamma} = \frac{\gamma\eta}{m^*}, \quad \dot{\eta} = \frac{1}{m^*}\left(\frac{4}{\gamma^4} - \eta^2\right) + \frac{4\omega_{\mathrm{I}}}{\gamma^3}, \tag{29}$$

where $t \to t/2|\Omega_{\mathrm{T}}|$ and $m^* = 2|\Omega_{\mathrm{T}}| d^2 M^*/\hbar$ are dimensionless time coordinate and polariton mass, respectively, $\omega_{\mathrm{T}} = \mathrm{sgn}(\Omega_{\mathrm{T}})$, $\omega_{\mathrm{I}} = \Omega_{\mathrm{I}}/(4\sqrt{\pi}|\Omega_{\mathrm{I}}|)$.

Phase diagrams for various dynamical regimes are determined by the property of polariton mass m^* and by the sign of Hamiltonian H that is supposed to be a conserved quantity. In particular, at $m^* > 0$ a polariton wave packet exhibits diffusive and self-trapping regimes for which $\gamma \to \infty$, $\eta \to 0$ and $\gamma \to const$, $\eta \to \infty$ at large, and in the limit case – at infinite, time scales ($t \to \infty$), respectively.

A phase diagram of a polariton wave packet is richer in the case of a negative polariton mass, i.e. at $m^* < 0$. In this case, the sign of the Hamiltonian function H becomes important, and in dimensionless coordinates, it looks like:

$$H = -\omega_{\mathrm{T}} \cos(p)\, e^{-\sigma} + \frac{\omega_{\mathrm{I}}}{\gamma}. \tag{30}$$

The transition between different regimes occurs at $H = H_0 = 0$, which implies $\cos(p) \simeq 0$; we denote H_0 as the initial value of Hamiltonian H which is, obviously, a conserved quantity in the absence of dissipation.

A physically important bound state for our problem occurs in the domain of negative polariton mass ($m^* < 0$) and this can be associated with the soliton formation for a polariton wave packet. The polariton (bright) soliton wave packet propagates with the initial width $\gamma_0 \equiv \gamma(t = 0)$, mass $m^* = m_0^* < 0$ and velocity $v_g = -\tan(p_0)/|m_0^*|$ being unchanged in time. The mass of a soliton wave packet can be found from:

$$\frac{1}{m_0^*} = \omega_{\mathrm{T}} \cos(p_0)\, e^{-\sigma_0}. \tag{31}$$

Strictly speaking, Eq. (31) defines a characteristic domain of the allowed wave packet momentum where solitonic regime can be achieved. In particular, this domain is determined by characteristic values of the polariton momentum which obeys the inequality $\cos(p) < 0$ that corresponds to the physical situation described in [17] for atomic BEC lattice solitons.

5. Polariton wave packet dynamics

For further analysis, it is much better to regard special cases which reflect physical features of polaritons in the lattice. In Fig. 2, we build a phase diagram for various dynamical regimes of the polariton wave packet formation in the lattice. In particular, according to our analysis of Eqs. (29)–(31), we deal with only two domains defined for $\cos(p_0) > 0$ and $\cos(p_0) < 0$ respectively. To be more specific, we suppose that $\Omega_{\mathrm{T}} > 0$, i.e. $\omega_{\mathrm{T}} = 1$.

In Fig. 2a, we plotted trajectories in the $\gamma - \eta$ plane which are relevant to the area where $\cos(p_0) > 0$. Such trajectories can be found by using the equation for energy conservation, i. e. $H = H_0$ which implies that:

$$\eta = \frac{2}{\gamma}\left(2\ln\left[\frac{\gamma^2\cos(p_0)}{\gamma\omega_{\mathrm{I}} - H_0\gamma^2}\right] - \frac{1}{\gamma^2}\right)^{1/2}. \tag{32}$$

From (32), when $H_0 > 0$, we can obtain the maximal the value of the wave packet width $\gamma_{\max} = \frac{\omega_{\mathrm{I}}}{H_0}$ for which a self-trapping regime is realized. Actually, in this case, polariton group velocity v_g and effective mass m^* are limited by the value $v_g \simeq \frac{\tan(p_0)}{m^*}$ with mass $m^* = \sec(p_0)\exp\left\{\frac{\gamma_{\max}^2\eta^2}{8} + \frac{1}{2\gamma_{\max}^2}\right\}$, respectively.

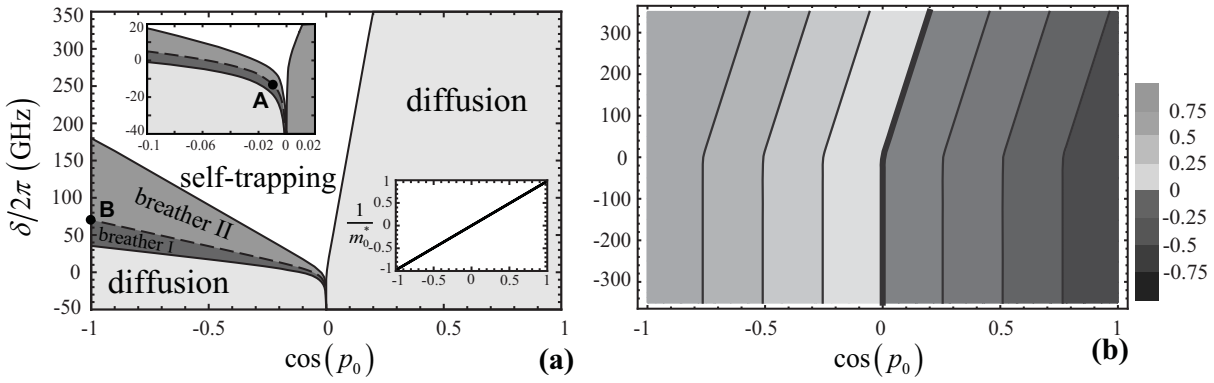

Fig. 2. (a) – Dynamical phase diagram in $\delta - \cos(p_0)$ plane, and, (b) – relevant Hamiltonian contour for $d = 4\mu$m. Initial conditions are: $\gamma_0 = 5$, $\eta_0 = 0$. The right inset shows the behavior of inverse polariton mass $1\,/\,m_0^*$ versus $\cos(p_0)$. The dashed curve corresponds to the soliton regime and separates two breathing domains, respectively

Asymptotic properties of the wave packet at infinite time ($t \to \infty$) for which $\eta \gg 1$ implies that LB polaritons in the cavity array can be fully stopped, i.e. $v_g \to 0$ when the effective mass goes to infinity, i. e. $m^* \to \infty$, see Fig. 3a.

Now, let us consider the limit of the negative Hamiltonian, that is $H_0 < 0$. At long times, i. e. for $t \gg 1$ the width is $\gamma \gg 1$; the LB polariton wave packet spreads with

mass $m^* \approx 1/|H_0|$ and parameter $\eta \approx \frac{2}{\gamma}\sqrt{2\ln[m^*\cos(p_0)]} \equiv \eta_{\rm D}$, that corresponds to the *diffusive regime* of polariton wave packet propagation.

In practice, it is more convenient to change atom-light detuning δ for tuning polariton-polariton scattering parameters. In this case, the equation $H_0 = 0$ defines some critical value $\delta_{\rm C}$ of atom-field detuning for which transition between different regimes occurs – see Fig. 3a. Analytically, it is easy to elucidate a polariton behavior for small values of the momentum parameter $\cos(p_0)$. In this case, the critical value of $\delta_{\rm C}$ can be inferred from the equation $\frac{\omega_{\rm I}}{\gamma_0} = |\cos(p_0)|\, e^{-\sigma_0}$. Since the atom-field coupling parameter g is essentially smaller than the photon tunneling rate α for the appropriate experimental situation, the equation under discussion permits only negatively defined solutions for δ. In other words, in this limit, we deal with photon-like polaritons for which modulus of critical detuning $\delta_{\rm C}$ approaches

$$|\delta_{\rm C}| \simeq \left(\frac{g^4 N_{\rm pol} e^{\sigma_0}}{2\sqrt{\pi}\gamma_0 |\cos(p_0)|\,\alpha N}\right)^{1/3}, \tag{33}$$

where we suppose that condition $g \ll |\delta|$ is satisfied.

Now we suppose that the initial wave packet momentum obeys to a condition $\cos(p_0) < 0$, which implies initially negative polariton mass, Fig. 3a. Analysis of different regimes can be performed by using the initial value of Hamiltonian $H_0 = \frac{1}{|m_0^*|} + \frac{\omega_{\rm I}}{\gamma_0}$ which is certainly positive – see Fig. 3b. By using the energy conservation law $H_0 = H$, it is easy to determine if $H_0 > |\cos(p_0)|$, a wave packet width remains finite and we deal with localized polariton states, i.e. with self-trapping or breathing regimes. Conversely, the diffusive regime with $\gamma \to \infty$ and $\eta = \eta_{\rm D}$ occurs if $H_0 < |\cos(p_0)|$.

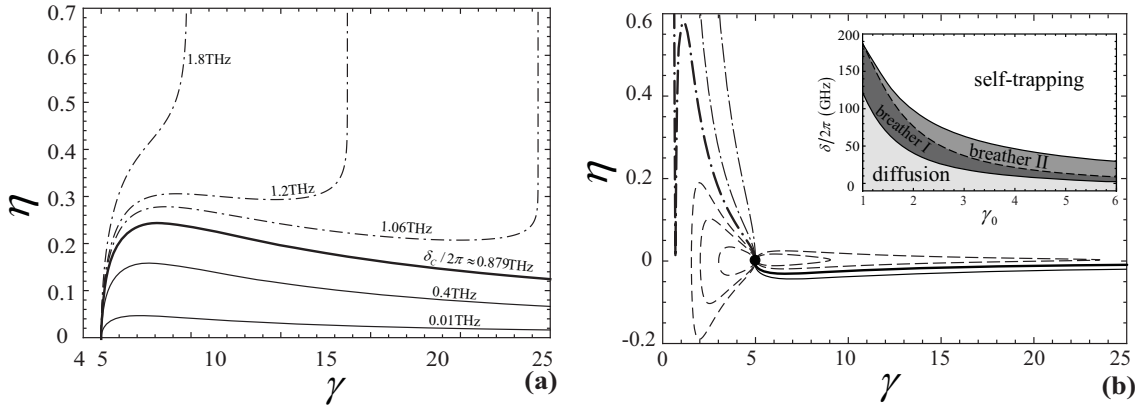

Fig. 3. Trajectories in the $\eta - \gamma$ plane for various atom-field detuning δ in the case where (a) – $\cos(p_0) > 0$ and, (b) – $\cos(p_0) < 0$. The initial values of the wave packet width and curvature are $\gamma_0 = 5$, $\eta_0 = 0$, respectively. Other parameters are: $d = 4\mu$m, $\cos(p_0) = 0.5$ for (a), and, $\cos(p_0) = -0.2$ for (b). In the inset the dependence of δ on γ_0 for $\cos(p_0) = -0.2$ is plotted. The magnitudes of $\delta/2\pi$ beginning with the bottom line in (b) are: -10GHz, $\delta_{\rm C}/2\pi \approx 5.112$GHz (bold curve) for solid curves, respectively; 7.1GHz, 10GHz and 18GHz, 23GHz, 27GHz for dashed curves, respectively; $\delta_{\rm BR}/2\pi \approx 36.138$GHz (bold dashed-dotted curve); 60GHz and 200GHz for dashed-dotted curves, respectively. The black dot in (b) corresponds to the solitonic regime of wave packet parameters obtained at $\delta_{\rm S}/2\pi \approx 13.422$GHz

The transition between the discussed physical situations is characterized by the condition $H_0 = |\cos(p_0)|$. Thus, polaritons with detuning $\delta < \delta_{\rm C}$ undergo a diffusive regime for which we asymptotically have $\gamma \to \infty$ and $\eta \to 0$.

If atom-field detuning belongs to $\delta_{\rm C} < \delta < \delta_{\rm S}$ domain, the first breathing regime can be obtained. The trajectories in $\eta - \gamma$ space are closed; the effective mass $m^*(t)$ and $\gamma(t)$ oscillating in time. The latest one oscillates between the initial value γ_0 and the value $\gamma_{\max}^{\rm osc}$, that is $\gamma_{\max}^{\rm osc} > \gamma_0$. For atom-field detuning chosen from the second breathing region $\delta_{\rm S} < \delta < \delta_{\rm BR}$, parameters $\gamma(t)$ and $\eta(t)$ also undergo temporal oscillations. However, in this case, the width $\gamma_{\min}^{\rm osc}$ of a polariton wave packet is limited by the initial value γ_0, that is $\gamma_{\min}^{\rm osc} < \gamma_0$.

Frequencies $\omega_{\rm BR\,1,2}$ of small amplitude oscillations of the wave packet width γ for the above discussed breathing regimes could be easily found by linearizing Eqs. (29) around some average values $\gamma_{1,2}$, and have the form:

$$\omega_{\rm BR\ 1,2} = \left[\frac{8\omega_{\rm I}}{\gamma_{1,2}^3}\left(\frac{1}{\gamma_{1,2}^2} - 1\right)|\cos(p)| - \frac{4}{\gamma_{1,2}^4}\left(\frac{5}{\gamma_{1,2}^2} - 3\right)|\cos(p)|^2\right]^{1/2}, \qquad (34)$$

where indexes "1" and "2" are relevant to two types of breathing regimes, respectively.

The dashed curve in Fig. 2a (see also inset to Fig. 3b), which corresponds to detuning $\delta_{\rm S}$ and separates two breathing regimes, characterizes bright soliton solution of Eqs. (29) taken for $\dot{\gamma} = 0$, $\eta = 0$.

On the other hand, a half-matter–half-photon polariton soliton with $\delta_{\rm S} = 0$ propagates in the cavity array with momentum $p_0 \simeq \left|\arccos\left(\frac{gN_{\rm pol}\gamma_0 e^{\sigma_0}}{4\sqrt{\pi}\alpha N}\right)\right|$.

Finally, if $\delta > \delta_{\rm BR}$, a polariton self-trapping regime is established. However, apart from the case of $\cos(p_0) > 0$ in this limit one can obtain $\gamma \to \gamma_{\min} < \gamma_0$ with $\eta \to \infty$.

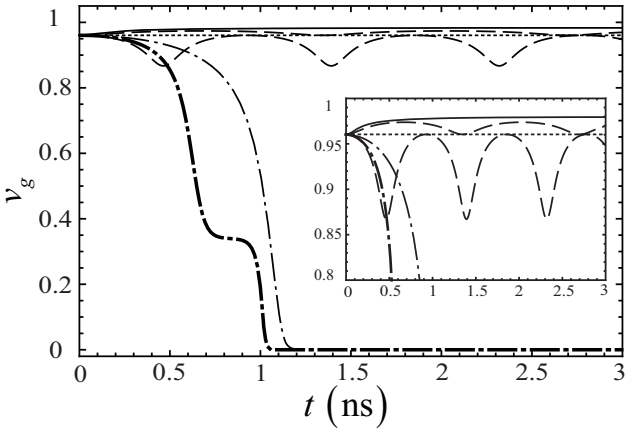

Fig. 4. Polariton wave packet group velocity v_g versus time t for $\gamma_0 = 5$, $\cos(p_0) = -0.2$. Beginning from the top of the figure, $\delta/2\pi = \delta_{\rm C}/2\pi \approx 5.112$GHz and $v_0 \equiv v_g(t=0) = 2888030$m/s (solid curve); 10GHz and $v_0 = 2150090$m/s (upper dashed curve); $\delta/2\pi = \delta_{\rm S}/2\pi \approx 13.421$GHz and $v_0 = 1630070$m/s (dotted line); 23GHz and $v_0 = 812925$m/s (lower dashed curve); $\delta/2\pi = \delta_{\rm BR}/2\pi \approx 36.138$GHz and $v_0 = 387474$m/s (dashed-dotted bold curve); 60GHz and $v_0 = 152560$m/s (dashed-dotted curve)

Figure 4 demonstrates typical temporal dynamics of the wave packet group velocity v_g in the discussed case. For detuning $\delta < \delta_{\rm C}$, we deal with the diffusive regime for which a group velocity tends to the constant value $v_g \approx \sin(p_0)$ asymptotically. On the other

hand, a group velocity oscillates in time within the window $\delta_{\rm C} < \delta < \delta_{\rm BR}$ (small-amplitude oscillations of the group velocity are shown in the inset in Fig. 4). For $\delta > \delta_{\rm BR}$, i.e. for a self-trapping regime, v_g rapidly vanishes and goes to zero. The soliton regime is established for atom-field detuning $\delta = \delta_{\rm S}$ and is obviously characterized by a constant value of the group velocity – dotted line in Fig. 4.

6. Physical algorithm of storing of photonic information

Different regimes obtained in the paper enable us to use them for the quantum optical information storage with the help of LB polariton solitons. As an example, here we establish a physical protocol of optical information storage by using specific points **A** and **B** in the phase diagram represented in Fig. 2, these points corresponding to polariton soliton formation. Physical principles of our protocol are established in Fig. 5. The protocol is based on the manipulation with a group velocity of photonic field (polariton mass) in the cavity array which has been discussed in detail in Sec. 4. In particular, at the first (writing) stage a photonic wave packet should enter a cavity array completely. In this case, LB polaritons are photon-like ($\Xi_{2,n} \propto \psi_n$) with mass $M^* \approx m_{\rm ph}$. Initially, soliton parameters that correspond to point **A** in Fig. 2a were given by the values $\cos\left(p_0^{\rm ph}\right) = -0.01$, $\delta \equiv \delta_{\rm ph} \approx -2\pi \times 12.763$GHz, respectively. Then, we should switch atom-filed detuning to magnitude $\delta \equiv \delta_{\rm at} \approx 2\pi \times 70.328$GHz and choose LB polariton momentum as $\cos(p_0^{\rm at}) = -1$ for mapping optical information into coherent matter excitations. This situation is displayed in Fig. 2 by moving across the solitonic phase boundary toward point **B** that corresponds to matter-like LB polaritons ($\Xi_{2,n} \propto \phi_n$) with the mass $M^* \approx m_{\rm ex}$ posing low enough group velocity – see Fig. 4.

At the last stage the original wave packet can be reconstructed at the entrance of the cavity array. The time interval $\tau_{\rm R}$ corresponds to the restoration of optical information by using the process which is reversed with respect to detuning δ and momentum p_0. In the ideal case, we should obtain the same, photon-like polariton soliton wave packet as a result – see Fig. 5.

However, in the real world all time intervals characterizing writing, storing and retrieving stages for quantum memory purposes strictly depend on dissipation and decoherence effects with a coupled qubit-light system in the cavity array. The specifics of these effects that leads to diminishing quantum optical information storage fidelity depends on the peculiarities of a concrete realization of the system represented in Fig. 1. This important question requires separate analysis and this will be discussed elsewhere.

7. Conclusion

In this work, we consider the problem of lattice polariton soliton formation in the array of weakly coupled qubit ensembles interacting with the quantized photonic field in a tunnel-coupled cavity array – 1D lattice structure. Such cavities can be designed by using photonic crystal structures with the defects posing small (micro-scale) spatial sizes. We have demonstrated that this feature plays an essential role in the consideration of fundamental tunneling processes between cavities at different spatial scales. In particular, we focus on LB polariton wave packet properties obtained in the limit of strong qubit-light coupling condition and under the low temperatures when the upper polariton branch population can be neglected. We have shown that polariton wave packet exhibits four different dynamical regimes. First, there is a *diffusive regime* for which a polariton wave packet extends representing approximately a half matter–half photon quasi-particle state.

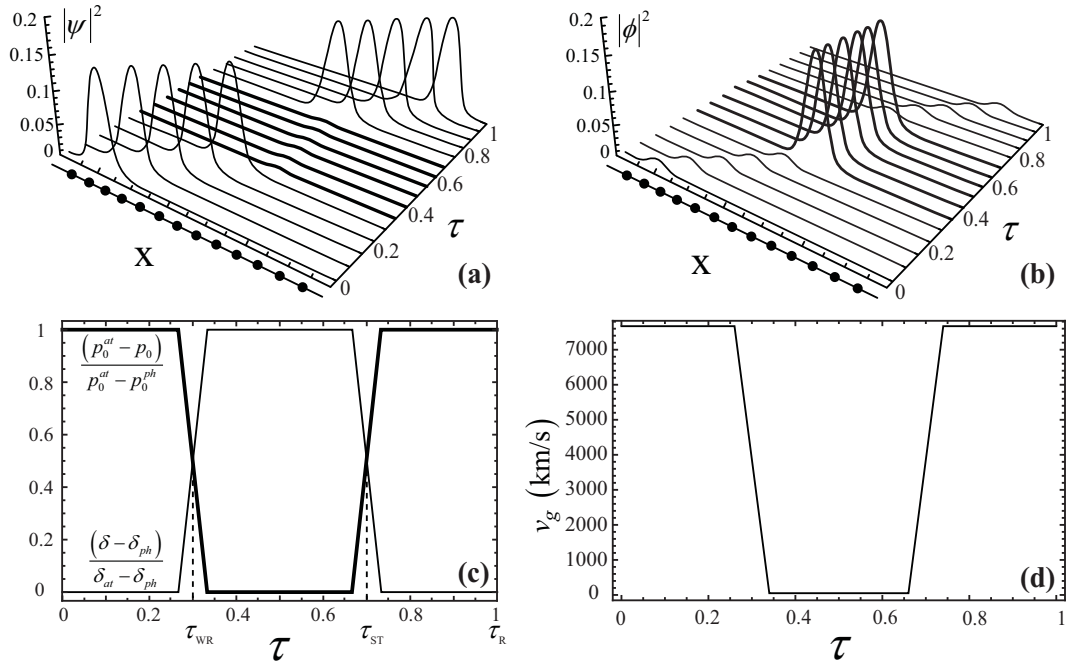

Fig. 5. Coherent spatio-temporal evolution of (a) – photonic ($|\psi|^2$) and, (b) – atomic excitation ($|\phi|^2$) components of the LB bright polariton soliton wave packet propagating in 1D cavity array (cavities are shown as bold points in x direction). The manipulation in time is realized by using scaled detuning δ and momentum p_0, respectively, shown in (c) and, by group velocity – (d). Axes are taken in arbitrary units

The second regime corresponds to intrinsically localized polaritonic modes; this is the so-called *breathing regime* when a wave packet moves with an oscillating width. Third, we deduce a *self-trapping regime* when a matter-like polariton wave packet can be stopped and localized within a few cavities only. Finally, we elucidate the regime of bright *polariton soliton* formation that corresponds to the propagation of the polariton wave packet in the lattice with constant velocity and its shape unchanged. One of the important features of the solitonic regime being under discussion is connected with the fact that it may be formed for both photon-like and matter-like domains of a coupled qubit-light system in the cavity array. Such a property of polariton solitons in our problem seems to be very attractive for the storage of quantum optical information.

In this paper we suggest a new physical algorithm for quantum optical memory which is based on the transformation and manipulation by polariton solitons in the cavity array. Although we do not examine any dissipation and quantum decoherence effects for a coupled qubit-light system considered in the paper, we hope that our approach opens new perspectives for quantum information processing with the help of polariton solitons containing a small particle number. Here, we would like to represent some arguments in favor of our point of view.

Obviously, the quantum optical information can be stored within the time interval that in practice depends on the qubit decoherence time and quality factor of a cavity array. One can expect that for the qubits based on the semiconductor QDs cavity QED array it is possible to achieve the storage time within tens of picoseconds domain with high enough

fidelity, [25]. Conversely, if we use two-level ultracold atoms, or NV-centers in diamonds as qubits we can operate with a memory device within tens of nanoseconds or more [26].

Second, our protocol of the optical information storage with the help of soliton states posses some important advantages with respect to other methods, which are based on the quantum information storage of operating other Gaussian-type optical pulses. In particular, solitons seem to be much more robust to small perturbations. Even in the presence of small dissipation and decoherence effects, it is possible to operate with a soliton-like shape, preserving wave packets in accordance with perturbation approach for polariton solitons, cf. [20].

Third, if dissipation and decoherence effects become significant, we hope that it will be possible to find some solitonic regimes for pulse propagation that corresponds to dissipation solitons. In this limit, solitons are formed due to some additional optical pumping. Quantum properties of such solitons and the fragility of their quantum states against decoherence and dissipation effects, which seem very important, especially for quantum optical information memory devices, can be optimized by using non-classical states for a pumping field, cf. [27].

Appendix: Estimation of tunneling coefficients for atomic system

Here, we discuss properties of parameters (11), (12) for the cavity-QED array containing two-level atoms as a qubit system. To be more specific, we consider ultracold two-level rubidium atoms with resonance frequency $\omega_{12} / 2\pi = 382\mathrm{THz}$ that corresponds to mean weighted rubidium *D*-lines. To get a variational estimate for the tunneling coefficients mentioned above, we assume that the Wannier wave functions for atomic and photonic parts localized at the *j*th cavity may be approached by (cf. [28]):

$$\varphi_{j,n}\left(\vec{r}\right) = C_j e^{\frac{-(x-x_n)^2}{2\sigma_{x,j}^2}} e^{\frac{-\left(y^2+z^2\right)}{2\sigma_j^2}}, \qquad \xi_n\left(\vec{r}\right) = C_\xi e^{\frac{-(x-x_n)^2}{2\xi_x^2}} e^{\frac{-\left(y^2+z^2\right)}{2\xi^2}}, \tag{A.1}$$

where $C_j = \left(\pi^{3/2}\sigma_{x,j}\sigma_j^2\right)^{-1/2}$ $(j = 1, 2)$, $C_\xi = \left(\pi^{3/2}\xi_x\xi^2\right)^{-1/2}$ are relevant normalization constants. Taking into account the realistic values of variational parameters $\sigma_{x,j}$, σ_j and ξ_x, ξ, which are widths of atomic and photonic wave functions, respectively, we assume that:

$$\sigma_{x,j} \ll \sigma_j, \quad \xi_x \ll \xi. \tag{A.2}$$

Here, we also propose some trapping of the atoms in the cavity. In the simplest case, we can choose harmonic trapping potentials $V_{\mathrm{exp}} = V_{\mathrm{opt}} + V_{\mathrm{m}}$ with components:

$$V_{\mathrm{m}} = \frac{M_{\mathrm{at}}}{2}\left(\omega_{\mathrm{mag},x}^2 x^2 + \omega_{\mathrm{mag},\perp}^2\left(y^2+z^2\right)\right), \quad V_{\mathrm{opt}} = sE_{\mathrm{R}}\sin^2\left(kx\right) \approx \frac{M_{\mathrm{at}}}{2}\omega_x^2\left(x-x_n\right)^2, \tag{A.3}$$

where $E_{\mathrm{R}} = \hbar^2k^2/2M_{\mathrm{at}}$ is recoil energy, $s = V_0/E_{\mathrm{R}}$ is a dimensionless parameter which denotes the lattice depth. We take a cylindrically symmetric trap potential with characteristic axial and radial frequencies $\omega_{\mathrm{mag},x}$ and $\omega_{\mathrm{mag},\perp}$ respectively. We suppose that the minima of the 1D periodic potential (A.3) are located at the centers $x_n = nd$ of nth cavity, i. e. $\omega_x = \left(2sE_{\mathrm{R}}k^2/M_{\mathrm{at}}\right)^{1/2}$. For the typical values of trapping frequencies $\omega_{\mathrm{mag},x}$ and ω_x, it is possible to obtain $\omega_x \gg \omega_{\mathrm{mag},x}$, cf, [28]. After substituting (A.1), for (11), (12) and taking into account (A.2), for the atomic tunneling rate β we obtain:

$$\beta = -\frac{\hbar}{4M_{\mathrm{at}}\sigma_x^2}e^{\frac{-d^2}{4\sigma_x^2}}\left(1-\frac{d^2}{2\sigma_x^2}\right) - \frac{M_{\mathrm{at}}\omega_x^2}{4\hbar}e^{\frac{-d^2}{4\sigma_x^2}}\left(\sigma_x^2+\frac{d^2}{2}\right). \tag{A.4}$$

In the experimental situation the second term in (A.4) is essentially smaller than the first one. Thus, we can assume that $\beta \approx -\frac{\hbar}{4M_{\rm at}\sigma_x^2} e^{\frac{-d^2}{4\sigma_x^2}} \left(1 - \frac{d^2}{2\sigma_x^2}\right)$. The atomic tunneling rate β is positive if the cavity effective size is $d > \sqrt{2}\sigma_x \approx 1.414\sigma_x$. The latest one ($\sigma_x$) is typically few hundred nanometers in real experiments [18].

A calculation of the photon tunneling rate α between the cavities can be given in the same way. In particular, we obtain:

$$\alpha = -\frac{\hbar}{4M_{\rm ph}\xi_x^2} e^{-\frac{d^2}{4\xi_x^2}} \left(1 - \frac{d^2}{2\xi_x^2}\right). \tag{A.5}$$

Since $M_{\rm at} \gg M_{\rm ph}$ the relation $|\alpha| \gg |\beta|$ is fulfilled for the relevant tunneling rates and we can assume that $\Omega_{\rm T} \simeq \alpha C^2$ in Eq. (21).

Acknowledgements

This work was supported by RFBR Grants No. 14-02-31443, and No. 14-02-97503 and by the Russian Ministry of Education and Science state task 2014/13. A. P. Alodjants acknowledges support from “Dynasty” Foundation.

References

[1] C. Simon, M. Afzelius, J. Appel, et al. Quantum memories. *Eur. Phys. J. D*, **58**, P. 1–22 (2010).
[2] N. S. Ginsberg, S. R. Garner and L. V. Hau. Coherent control of optical information with matter wave dynamics. *Nature*, **445**, P. 623–626 (2007).
[3] A. I. Lvovsky, B. C. Sanders and W. Tittel. Optical quantum memory. *Nature Phot.*, **3**, P. 706–714 (2009).
[4] K. Hammerer, A. S. Sorensen, E. S. Polzik. Quantum interface between light and atomic ensembles. *Rev. Mod. Phys.*, **82**, P. 1041–1093 (2010).
[5] M. Fleischhauer and M. D. Lukin. Quantum memory for photons: Dark-state polaritons. *Phys. Rev. A*, **65**, P. 022314 (2002).
[6] A. P. Alodjants, S. M. Arakelian, and A. Yu. Leksin. Storage of quantum optical information based on the intracavity polaritons under the BoseEinstein Condensation conditions. *Laser Physics*, **17**, P. 1432–1440 (2007).
[7] A. Kitaev. Fault-tolerant quantum computation by anyons. *Ann. Phys.*, **303**, P. 2–30 (2003); ibid D. Jaksch, P. Zoller. The cold atom Hubbard toolbox. **315**, P. 52–79 (2005).
[8] L. Jiang, G. K. Brennen, A. V. Gorshkov, et al. Anyonic interferometry and protected memories in atomic spin lattices. *Nature Phys.*, **4**, P. 482–488 (2008); A. J. Daley, J. Ye, and P. Zoller. State-dependent lattices for quantum computing with alkaline-earth-metal atoms. *Eur. Phys. J. D*, **65**, P. 207–217 (2011).
[9] A. Tomadin and R. Fazio. Many-body phenomena in QED-cavity arrays. *J. Opt. Soc. Am. B*, **27**, P. A130–A136 (2010); M. J. Hartmann, F. G. S. L. Brandao, and M. B. Plenio. Effective Spin Systems in Coupled Microcavities. *Phys. Rev. Lett.*, **99**, P. 160501 (2007).
[10] S.-C. Lei and R.-K. Lee. Quantum phase transitions of light in the Dicke-Bose-Hubbard model. *Phys. Rev. A*, **77**, P. 033827 (2008).
[11] D. G. Angelakis, M. F. Santos, and S. Bose. Photon-blockade-induced Mott transitions and XY spin models in coupled cavity arrays. *Phys. Rev. A*, **76**, P. 031805(R) (2007).
[12] C. Kittel, *Introduction to Solid State Physics*, 7th ed., Wiley, New York, 673 p. (1996).
[13] H. Deng, G. Weihs, D. Snoke, et al. Polariton lasing vs. photon lasing in a semiconductor microcavity. *PNAS*, **100**, P. 15318–15323 (2003).
[14] A. Amo, S. Pigeon, D. Sanvitto, et al. Polariton Superfluids Reveal Quantum Hydrodynamic Solitons. *Science*, **332**, P. 1167–1170 (2011).
[15] B. Nelsen, R. Balili, D. W. Snoke, et al. Lasing and Polariton Condensation: Two Distinct Transitions in GaAs Microcavities with Stress Traps. *J. Appl. Phys.*, **105**, P. 122414 (2009).
[16] M. Sich, D. N. Krizhanovskii, M. S. Skolnick, et al. Observation of bright polariton solitons in a semiconductor microcavity. *Nat. Photon.*, **6**, P. 50–55 (2012).

[17] A. Trombettoni and A. Smerzi. Discrete Solitons and Breathers with Dilute Bose-Einstein Condensates. *Phys. Rev. Lett.*, **86**, P. 2353–2356 (2001).

[18] J.-J. Wang, A.-X. Zhang, K.-Zh. Zhang, J. Ma, and J.-K. Xue. Two-component Bose-Einstein condensates in D-dimensional optical lattices. *Phys. Rev. A*, **81**, P. 033607 (2010); A.-X. Zhang and J.-K. Xue. Coherent matter waves of a dipolar condensate in two-dimensional optical lattices. *Phys. Rev. A*, **82**, P. 013606 (2010).

[19] A. P. Alodjants, I. O. Barinov, and S. M. Arakelian. Strongly localized polaritons in an array of trapped two-level atoms interacting with a light field. *J. Phys. B*, **43**, P. 095502 (2010); E. S. Sedov, A. P. Alodjants, S. M. Arakelian, Y. Y. Lin, and R.-K. Lee. Nonlinear properties and stabilities of polaritonic crystals beyond the low-excitation-density limit. *Phys. Rev. A*, **84**, P. 013813 (2011).

[20] I-H. Chen, Y. Y. Lin, Y.-C. Lai, et al. Solitons in cavity-QED arrays containing interacting qubits. *Phys. Rev. A*, **86**, P. 023829 (2012).

[21] M. Notomi, E. Kuramochi, and T. Tanabe. Large-scale arrays of ultrahigh-Q coupled nanocavities. *Nature Phot.*, **2**, P. 741–747 (2008); K. Hennessy, A. Badolato, M. Winger, et al. Quantum nature of a strongly coupled single quantum dotcavity system. *Nature*, **445**, P. 896–899 (2007).

[22] Q. J. Wanga, C. Yan, N. Yu, et al. Whispering-gallery mode resonators for highly unidirectional laser action. *PNAS*, **107**, P. 22407–22412 (2010).

[23] F. A. Zwanenburg, A. S. Dzurak, A. Morello, et al. Silicon quantum electronics. *Rev. Mod. Phys.*, **85**, P. 961–1019 (2012).

[24] A. Szameit, Th. Pertsch, S. Nolte, A. Tünnermann, and F. Lederer. Long-range interaction in waveguide lattices. *Phys. Rev. A*, **77**, P. 043804 (2008).

[25] N. Cody Jones, R. Van Meter, A. G. Fowler, et al. Layered Architecture for Quantum Computing. *Phys. Rev. X*, **2**, P. 031007 (2012).

[26] C.-H. Su, A. D. Greentree, and L. C. L. Hollenberg. Towards a picosecond transform-limited nitrogen-vacancy based single photon source. *Opt. Express*, **16**, P. 6240–6250 (2008); S. Castelletto, J. P. Harrison, L. Marseglia, et al. Diamond-based structures to collect and guide light. *New J. of Phys.*, **13**, P. 025020 (2011).

[27] A. Dantan, J. Cvilinski, M. Pinard and Ph. Grangier. Dynamics of a pulsed continuous-variable quantum memory. *Phys. Rev. A*, **73**, P. 032338 (2006).

[28] A. Trombettoni, A. Smerzi, and P. Sodano. Observable signature of the Berezinskii-Kosterlitz-Thouless transition in a planar lattice of Bose-Einstein condensates. *New J. of Phys.*, **7**, P. 57 (2005).